

# Demonstration of effective UCB-based routing in skill-based queues on real-world data

Sanne van Kempen, Jaron Sanders, Fiona Sloothaak, Maarten G. Wolf

## Abstract

This paper is about optimally controlling skill-based queueing systems such as data centers, cloud computing networks, and service systems. By means of a case study using a real-world data set, we investigate the practical implementation of a recently developed reinforcement learning algorithm for optimal customer routing. Our experiments show that the algorithm efficiently learns and adapts to changing environments and outperforms static benchmark policies, indicating its potential for live implementation. We also augment the real-world applicability of this algorithm by introducing a new heuristic routing rule to reduce delays. Moreover, we show that the algorithm can optimize for multiple objectives: next to payoff maximization, secondary objectives such as server load fairness and customer waiting time reduction can be incorporated. Tuning parameters are used for balancing inherent performance trade-offs. Lastly, we investigate the sensitivity to estimation errors and parameter tuning, providing valuable insights for implementing adaptive routing algorithms in complex real-world queueing systems.

## 1 Introduction

In skill-based queues, different customer types request service from a set of heterogeneous servers, and compatibility relations determine which customer-server matches are allowed. Since such systems are widely used in data centers, cloud computing networks, healthcare applications, and service systems, efficient resource allocation is highly valuable [1]. Full theoretical understanding of such systems, however, is challenging due to the complex queueing dynamics and compatibility relations [2, 3, 4].

Canonical routing policies such as (i) First-Come-First-Served (FCFS)—Assign-the-Longest-Idle-Server (ALIS), (ii) the  $c\mu$  rule, (iii) threshold-based policies, or (iv) Serve-the-Longest-Queue policy are typically static by design [3, 5]. Although such policies are easy to implement, they ignore long-term effects and/or stability constraints. Moreover, they offer limited robustness and adaptability to optimize for various objectives such as maximizing the quality of customer-server matches, waiting time, fairness, and server loads.

To address these challenges, there has been a growing interest in adaptive control policies that make data-driven decisions based on real-time feedback [6, 7, 8]. In particular, recent works underline the potential of machine learning algorithms for practical implementation in queueing systems. For example, [9] applies a proximal policy optimization for routing in a multiclass queueing networks, [10] optimizes congestion control in a data center using a reinforcement learning algorithm, [11] introduces an actor-critic method for job scheduling in a multi-resource job scheduling, and [12] introduces new score-aware gradient estimators which are applied in policy-gradient methods for stochastic optimal control problems.

Motivated by this, we focus on a recently developed utility-maximizing reinforcement learning algorithm, called “UCB-Queue Routing (UCB-QR)”, for routing in skill-based queues [13]. This algorithm integrates multi-armed bandit techniques and Upper Confidence Bounds (UCB) estimators in skill-based queueing systems [14, 15] to make routing decisions under uncertainty. It is shown that the algorithm is nearly optimal in the sense that its regret accumulation matches the asymptotic lower bound up to logarithmic terms. While the theoretical performance of UCB-QR has been analyzed in detail, its practical value in real-world queueing systems was not yet demonstrated. For example, queue lengths, delays, and fairness aspects of the algorithm are not considered in [13]. To this end, we perform an extensive numerical study of the potential applications and extensions for practical use of the algorithm in a realistic setting. We adapt the algorithm for implementation in a practical setting: this includes action space reduction and dealing with temporary system instability and time-varying arrival rates and service capacity. While these phenomena are often neglected in synthetic experiments, they are critical for realistic applications.

To prepare for potential implementation of the algorithm in a real-life setting, we provide with this paper a simulation framework designed to accommodate for generic queueing system configurations. This includes the

feature to set arbitrary compatibility relations and general arrival and service processes, making it a valuable tool for testing performance and robustness of learning-based routing policies in complex realistic environments. The simulation is made publicly available<sup>1</sup>. To demonstrate the practical use of the UCB-QR routing algorithm, we draw on data from a large-scale call center of a U.S. bank, made publicly available by the Technion laboratory for Service Enterprise Engineering (SEELAB)<sup>2</sup>.

We demonstrate that the modified UCB-QR routing algorithm (Algorithm 1) is well-suited for implementation in a large, realistic queueing system, even when the environment is subject to change. We focus on payoff maximization, where payoff models the quality of customer-server routings and is defined as the empirical ratio of successful service completions. We show that the UCB-QR algorithm successfully accumulates high payoff while learning the payoff parameters and estimating the (time-varying) arrival and service rates. In one representative scenario, our algorithm closes the optimality gap by over 70% when compared to naive random routing (see Figure 5). By also developing a new heuristic routing rule as a new subroutine for UCB-QR, customer waiting times can be reduced significantly. Moreover, we show that multiple objectives can be optimized simultaneously, with tuning parameters balancing the trade-offs. Lastly, the algorithm is not black-box nor computationally heavy: the algorithm’s runtime is comparable with those of other routing policies like FCFS—ALIS or random routing.

## 1.1 Experiment overview

To showcase the potential of the algorithm in real-world settings, we conduct a series of experiments, which we now briefly discuss. With this case study we achieve three main objectives, namely (i) implementation of a state-of-the-art reinforcement learning algorithm in a realistic large-scale service system (Experiment 1), (ii) extension and improvement of the algorithm to address practical objectives (Experiments 2–4), and (iii) evaluation of the adaptability and robustness of the algorithm (Experiments 5, 6). Along the way, we discuss insightful numerical results that can be of interest for future studies.

1. **Proof of concept.** We find that the UCB-QR algorithm consistently outperforms the benchmark policies in terms of payoff accumulation, including a “greedy” policy and a variant of the  $c\mu$  rule that is modified for payoff maximization [5]. The loss in payoff due to learning the payoff parameters and estimating the (time-varying) arrival and service rates is at most 2% when compared to the all-knowing payoff maximizing “oracle” policy.
2. **Alternative routing rule to decrease waiting times.** As our proposed UCB-QR routing algorithm primarily aims for payoff maximization, it typically leads to higher customer delays than benchmark non-adaptive routing policies. These waiting times can be improved by noting that the routing rule used in UCB-QR dispatches customers to servers according to prescribed routing rates (Algorithm 2). By replacing this subroutine by a new heuristic routing rule, we show that the waiting times can be reduced to the levels of more delay-friendly policies (e.g. FCFS—ALIS), while still maintaining high payoff accumulation. This heuristic routing rule (Algorithm 3) is inspired by the Join-the-Shortest-Queue- $K$  (JSQ- $K$ ) customer dispatching policy presented in [16].
3. **Combining different performance objectives.** When managing queues in practice, payoff maximization is rarely the only performance measure. Instead, other measures like customer waiting time, fairness, and server load can be of interest. We show how UCB-QR can be adapted to accommodate for multiple, possibly competing objective functions. A balance in the trade-off between the different objectives can be made by tuning a set of system parameters.
4. **Resilience in bursty scenarios.** In real-life scenarios, the customer arrival process can be affected by incidents, outages, or special events that lead to customer surges or bursty arrival processes. To demonstrate the robustness of our algorithm under such events, we simulate an incident scenario by adding artificial customer bursts on top of the regular arrival process from the data set. We observe that our learning-based algorithm achieves overall the highest cumulative payoff compared to the benchmark policies. Moreover, it recovers from the arrival surges in terms of waiting times, although it takes longer than the benchmark policies. This showcases the spirit of our approach: despite short-term surges, our algorithm focuses on the long-term optimization of customer—server matching quality.
5. **Robustness against estimation errors.** Instead of assuming fixed and known arrival and service rates, the UCB-QR algorithm uses online estimators. We investigate in what way the accuracy of the estimators influences the algorithm’s performance. Our results indicate that empirical estimators work sufficiently

<sup>1</sup>See <https://github.com/SannevanKempen/UCBQR>.

<sup>2</sup>See <https://seelab.net.technion.ac.il/data/>.

well, and relatively little performance benefit can be gained by using the true parameter values for the arrival and service rate.

6. **Balancing reactivity and complexity.** UCB–QR learns the payoff parameters in an episodic structure: the payoff, arrival rate, and service rate estimators are updated at the start of each episode using observed samples from previous episodes. The episode length therefore controls the learning rate: the shorter the episodes, the faster the payoff parameters are learned. However, there exists a trade–off with computational complexity, since computations need to be performed at each episode. The episode length should therefore be small enough to capture the changes in the time-varying customer arrival rate, since otherwise customer waiting times become large. In our experimental setting, we find that the effect of the episode length on payoff accumulation is small.

## 1.2 Paper outline

The modified UCB–QR algorithm is presented in Section 2. Implementation challenges are discussed in Section 3, and experimental results are discussed in Section 4. Lastly, we conclude briefly in Section 5.

## 2 Algorithm description

We consider a skill-based queueing system with customer types  $\mathcal{I} = \{1, \dots, I\}$ , servers  $\mathcal{J} = \{1, \dots, J\}$ , and a set of compatibility lines connecting customer types and servers  $\mathcal{L} = \{(ij) : i \in \mathcal{I}, j \in \mathcal{J}\}$ . Customers wait in the queue of their type until they start service at one of the compatible servers. Each service completion of a type- $i$  customer at server  $j$  generates a random Bernoulli payoff with mean  $\theta_{ij} \in [0, 1]$ .

We present a modified version of the routing algorithm developed by [13], called UCB–QR, in Algorithm 1. The goal of UCB–QR is to maximize the total average payoff  $\sum_{(ij) \in \mathcal{L}} \theta_{ij} \mathbb{E}[D_{ij}(t)]$ , where  $\mathbb{E}[D_{ij}(t)]$  is the number of type- $(ij)$  departures, while learning the payoff parameter  $\theta_{ij}$  and maintaining queue stability. Algorithm 1 considers the following optimal transport linear program (LP) that optimizes the routing rates  $x_{ij}$  of type- $i$  customers to server  $j$  to maximize the total average payoff (1a). Constraint (1b) guarantees that all customers are routed to some server, and constraints (1c) restricts that the total server load  $\sum_{ij} x_{ij} / \mu_{ij}$  does not exceed  $1 - \varepsilon$  for some  $\varepsilon \in (0, 1)$ , ensuring stability of the queueing system.

$$\text{LP}(\lambda, \mu, \theta, \varepsilon) : \max_{x \geq 0} \sum_{(ij) \in \mathcal{L}} \theta_{ij} x_{ij}, \quad (1a)$$

$$\text{s.t.} \quad \sum_{j \in \mathcal{S}_i} x_{ij} = \lambda_i, \quad \forall i \in \mathcal{I}, \quad (1b)$$

$$\sum_{i \in \mathcal{C}_j} \frac{x_{ij}}{\mu_{ij}} \leq 1 - \varepsilon, \quad \forall j \in \mathcal{J}. \quad (1c)$$

Algorithm 1 divides the time horizon into episodes. At the start of episode  $k$ , the estimators for (i) the average payoffs  $\hat{\theta}_{ij}^k$ , (ii) the arrival rates  $\hat{\lambda}_i^k$ , and (iii) the service rates  $\hat{\mu}_{ij}^k$  are updated using collected samples. For the payoff parameters, UCB estimators [14, 15] are used which are updated in (5). Consequently, the set of routing rates  $x_{ij}$ ,  $(ij) \in \mathcal{L}$  are chosen such that the value of  $\text{LP}(\hat{\lambda}^k, \hat{\mu}^k, \hat{\theta}^k, \varepsilon)$  is maximized. During the episode, customers are then routed to servers according to the rates  $x$ . To implement this routing rule, virtual queues are used (Algorithm 2).

Algorithm 1 is an adaptation of the routing algorithm introduced in [13]. Inherent to real-life situations, not all assumptions made in [13] are satisfied in practical systems. We briefly discuss the most significant changes to make the algorithm suitable for practical implementation.

- **Action space reduction.** The algorithm described in [13] considers the set of all Basic Feasible Solutions (BFSs) of the LP as its action space, i.e., the set of candidate solutions. Each episode, the algorithm chooses the solution (action) with the highest estimated payoff based on the UCB estimators  $\hat{\theta}$ . Since the number of BFSs scales exponentially with the number of customer types  $I$ , servers  $J$ , and lines  $|\mathcal{L}|$ , this approach can be computationally prohibitive for large queueing systems. To reduce the complexity of the algorithm, we instead solve (1) directly at the start of each episode using current payoff estimates, and use its maximizer as the desired routing rates (Line 5). This approach avoids the need to enumerate or store the full set of BFSs. For fixed values  $\lambda, \mu, \theta, \varepsilon$ , (1) can be solved efficiently by modern solvers that rely on, e.g., the simplex method or interior-point methods [17], making this a scalable alternative.

- **Stability.** In [13], a notion of stability is assumed, which assures that (1) is feasible. However, (1) can be infeasible if the arrival volume of certain customer types exceeds the service capacity of its compatible servers. In practice, such situations are to be expected in real-life queueing systems, where temporary overloads can occur. In addition, estimation errors in  $\hat{\lambda}$  and  $\hat{\mu}$  can also lead to infeasibility of (1). In case (1) is infeasible under the estimated  $\hat{\lambda}$  and  $\hat{\mu}$ , we consider the following alternative LP:

$$\text{LP}^a(\lambda, \mu, \theta, \varepsilon) : \max_{x \geq 0} \sum_{(ij) \in \mathcal{L}} \theta_{ij} x_{ij} - \sum_{i \in \mathcal{I}} p x_{iz}, \quad (2a)$$

$$\text{s.t.} \quad \sum_{j \in \mathcal{S}_i} x_{ij} + x_{iz} = \lambda_i, \quad \forall i \in \mathcal{I}, \quad (2b)$$

$$\sum_{i \in \mathcal{C}_j} \frac{x_{ij}}{\mu_{ij}} \leq 1 - \varepsilon, \quad \forall j \in \mathcal{J}. \quad (2c)$$

LP<sup>a</sup> introduces a new fictitious “rejection” server  $z$  with infinite capacity and connections to all customer types. Part of the arrival rate  $\lambda_i$  of customer  $i$  can be routed to server  $z$ , which is managed by the decision variables  $x_{iz}$ , but this is penalized in the objective by a negative payoff  $p$ . If the penalty  $p$  is large, then weight is given to  $x_{iz}$  only when there is no other feasible solution. This modified LP is always feasible and provides a robust alternative when (1) is infeasible. We note that the fictitious rejection server is not actually used when making routing decisions: after we obtain the optimal solution  $x$  from (2), we compute routing probabilities  $p_{ij}$  by normalizing the rates according to  $p_{ij} = x_{ij} / \sum_{k \in \mathcal{I}} x_{ik}$ , where server  $z$  is excluded (see Line 1 in Algorithm 1).

- **Arrival and service processes.** In [13], type- $i$  customers are assumed to arrive according to independent Poisson processes with known rates  $\lambda_i > 0$ , and service times are assumed to be independent and exponentially distributed with known rates  $\mu_j > 0$ . Since there is uncertainty and time-varying behavior in arrival rates and service capacity in real-life queueing systems, we use estimators (Line 3). This introduces more noise in the estimation errors that needs to be dealt with efficiently. The estimators  $\hat{\lambda}$  and  $\hat{\mu}$  are discussed in more detail in Section 3.1.4 and Section 3.1.3, respectively.

The pseudocode for our modified UCB–QR algorithm is shown in Algorithm 1 below.

---

**Algorithm 1** Modified UCB–Queue Routing (UCB–QR).

---

- 1: Initialize  $k = 1$ . For all  $(ij) \in \mathcal{L}$ , initialize  $T_{ij}(0) = \bar{\theta}_{ij}(0) = 0$  and  $\hat{\theta}_{ij}(0) = \infty$ .
- 2: **for** each episode  $k = 1, 2, \dots$  of length  $h$  **do**
- 3:   Set  $\hat{\lambda}^k$  according to (10) and  $\hat{\mu}^k$  according to (6).
- 4:   **if** LP( $\hat{\lambda}^k, \hat{\mu}^k, \hat{\theta}^k, \varepsilon$ ) (1) if feasible **then** ▷ Determine routing rates.
- 5:     Solve LP( $\hat{\lambda}^k, \hat{\mu}^k, \hat{\theta}^k, \varepsilon$ ) in (1); denote its maximizer by  $\hat{x}^k$ .
- 6:   **else**
- 7:     Solve LP<sup>a</sup>( $\hat{\lambda}^k, \hat{\mu}^k, \hat{\theta}^k, \varepsilon$ ) in (2); denote its maximizer by  $\hat{x}^k$ .
- 8:   **end if**
- 9:   Serve customers according to  $\hat{x}^k$  by applying Algorithm 2: FCFS–RR( $\hat{x}^k, h$ ). ▷ Route customers.
- 10:   For each line  $(ij) \in \mathcal{L}$ , observe  $N_{ij}^k \in \mathbb{N}_{\geq 0}$  payoff samples  $(Y_{ij}^\ell)_{\ell=1, \dots, N_{ij}^k}$ .
- 11:   For each line  $(ij) \in \mathcal{L}$ , update ▷ Update estimators based on samples.

$$T_{ij}(k) = T_{ij}(k-1) + N_{ij}^k, \quad (3)$$

$$\bar{\theta}_{ij}(k) = \frac{\bar{\theta}_{ij}(k-1)T_{ij}(k-1) + \sum_{\ell=1}^{N_{ij}^k} Y_{ij}^\ell}{T_{ij}(k)}, \quad (4)$$

$$\hat{\theta}_{ij}^k = \begin{cases} \bar{\theta}_{ij}(k) + \sqrt{\frac{\ln(k)}{T_{ij}(k)}} & \text{if } T_{ij}(k) > 0, \\ \infty & \text{if } T_{ij}(k) = 0. \end{cases} \quad (5)$$

12: **end for**

---

---

**Algorithm 2** FCFS-RR( $x, h$ ).

---

- 1: Set  $p_{ij} = x_{ij} / \sum_{k \in \mathcal{J}} x_{ik}$  for all  $(ij) \in \mathcal{L}$ . ▷ Compute routing probabilities.
  - 2: Empty all virtual queues. ▷ Shuffle virtual queues.
  - 3: For each waiting type- $i$  customer, assign it to the virtual queue of server  $j$  with probability  $p_{ij}$ .
  - 4: For each  $j \in \mathcal{J}$ , order the customers in virtual queue  $j$  by their arrival time.
  - 5: **for** time  $t = 0, \dots, h$  **do** ▷ Route customers.
  - 6:     **for** each arrival of a type- $i$  customer at time  $t$  **do**
  - 7:         Assign customer to the virtual queue of server  $j$  with probability  $p_{ij}$ .
  - 8:         If the server is idle, start service.
  - 9:     **end for**
  - 10:    **for** each service completion at server  $j$  at time  $t$  **do**
  - 11:         Obtain a payoff  $Y_{ij} \sim \text{Bern}(\theta_{ij})$ , where  $i$  is the departing customer’s type.
  - 12:         If the virtual queue of server  $j$  is non-empty, start service of the customer at the head of the queue.
  - 13:    **end for**
  - 14: **end for**
- 

### 3 Algorithm implementation

In this section we discuss the challenges that we encountered while implementing Algorithm 1. Although these preparatory steps are required for implementation of the algorithm, it is not strictly necessary to gain full understanding before reading the main results in section 4. The data set, necessary data preparation and a brief overview of the simulation setup are discussed in A.

#### 3.1 Implementation challenges

We split the data into training and testing data. The first two months of the data set, April and May 2001, will be used as training set to tune model parameters. All other months are used as testing data for the experiments in Section 4.

##### 3.1.1 Defining payoff parameters

To apply Algorithm 1, we need to define payoff parameters  $\theta_{ij}$  for the compatible lines  $(ij)$ . Since there are no measures of costs or customer satisfaction scores associated with this data set, we instead define a payoff based on service outcomes. In the data set, each call has an outcome label, including “transfer”, where a customer is transferred to an agent of another agent group, and “conference”, where the agent consults a second agent or supervisor. In both cases, the outcome indicates that additional resources were necessary to handle the call. We therefore define  $\theta_{ij}$  as the ratio of successful type- $(ij)$  services, i.e., services that do not end in transfer or a conference. Concretely, for a particular day  $d$  we let  $\theta_{ij}^d := s_{ij}^d / n_{ij}^d$  where  $s_{ij}^d$  is the number of type- $i$  calls that are routed to agent  $j$  on day  $d$  in the data set and do not end in transfer nor a conference, and  $n_{ij}^d$  is the total number of  $(ij)$  calls on day  $d$ . Note that the value of  $\theta$  thus depends on the day.

##### 3.1.2 Time-varying agent populations

In the data set, each agent group consists of several agents (see Table 1 for an example). For simplicity, we use one server for each agent group in the simulation. The service speed of each server is then scaled proportionally to the number of working agents in the data. This approximation can be considered similar to approximating an  $M(\lambda)/M(\mu)/n$  queueing system by an  $M(\lambda)/M(n\mu)/1$  system. Between these systems, the stationary probabilities are very close for states with  $n$  or more customers [18]. The data set contains the work hours of individual agents, including the duration spent answering calls or being available. For simplicity, we choose to update the number of available agents in the simulation every hour. For each hour, we obtain from the data the total number of agents per group that worked anytime during that hour.

Agent group	Agents
1	199
2	192
6	33
8	35
9	43
11	42
14	21
18	67
⋮	⋮

Table 1: Number of working agents per agent group on Tuesday May 1, 2001.

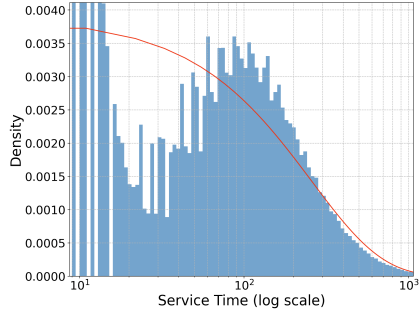


Figure 1: Histogram of type-(11) service times in May 2001 based on 252,103 samples, along with the density of an exponential distribution with parameter 257.

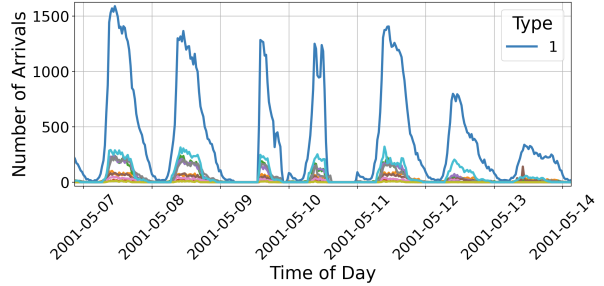


Figure 2: Number of customer arrivals accumulated per 30-minute intervals for the first week of May 2001. The call center is closed on the morning of May 9 and the afternoon of May 10.

### 3.1.3 Service time distribution

In Algorithm 1 we have to specify the service rate  $\hat{\mu}_{ij}^k$  for all lines  $(ij) \in \mathcal{L}$ . [13] assumes independent and exponentially distributed service times, but the service times in the data are unlikely to be actually distributed as such. For example, Figure 1 shows the empirical distribution of service times of type-1 customers at agent group 1 in May 2001, along with the best fitting exponential distribution. Here, “best” is measured in terms of the Akaike Information Criterion (AIC).

In order to make the simulation as close to the reality as possible, the service times of type- $i$  customers at server  $j$  in the simulation are sampled from the empirical distribution of the data set from that month. We define the service rate estimator  $\hat{\mu}_{ij}^k$  in Line 3 as the inverse of the empirical mean durations of type- $(ij)$  services that have been completed before the start of episode  $k$ , i.e.,

$$\hat{\mu}_{ij}^k := \frac{M_k}{\sum_{\ell=1}^{M_k} m_{ij}^{\ell}}, \quad (6)$$

where  $M_k$  is the number of type- $(ij)$  service completions up to episode  $k$ , and  $(m_{ij}^{\ell})_{\ell=1}^{M_k}$  are the realized service times of those completions.

### 3.1.4 Time-varying arrivals

Algorithm 1 takes as input the arrival rate of customers, i.e., the expected number of arrivals per time unit. The customer arrival rate in the call center is time-varying. For example: the number of calls at night is lower than during the day time; during office hours there is usually a peak in call volume at the start of the work day; and on weekends and holidays the number of calls is less than on an average weekday. The arrival pattern for one week is shown in Figure 2. We observe that type-1 customers dominate the customer population, which is consistent throughout the entire data set. For the simulation input, we use the actual arrival times as reported in the data set.

**Forecasting methods.** To solve (1), we use time-dependent estimators  $\hat{\lambda}^k$  that are updated at the start of each episode  $k = 1, \dots$ . Estimator  $\hat{\lambda}_i^k$  forecasts the arrival rate of type- $i$  customers in the next episode. There are many different methods for time series forecasting [19, 20, 21, 22]. Some methods, including the Holt–Winters’ seasonal method and (S)ARIMA and its extensions (e.g. SARIMAX), forecast the call volume for an entire day based on historical daily or seasonal patterns [19]. For example, the SARIMA relies on autoregression, temporal differencing and moving averages and takes seasonality into account. However, these methods tend to rely heavily on the assumption that the future follows the same overall structure as the past, and they can perform poorly when the system exhibits abnormal behavior on otherwise regular (non-holiday) days. Since (S)ARIMA models are typically fitted to longer-term daily or weekly cycles, they may not adapt quickly to unexpected fluctuations during the day, such as sudden surges in call volume due to external events, technical issues, or minor schedule changes. To make our forecasting more robust to such variations, we instead forecast the arrival rate using only the data of the day itself. This allows the model to react faster to deviations from typical patterns while still accounting for underlying trends. A wide range of such methods exist in literature, such as for example Generalized Additive Models and Bayesian Additive Regression Trees. For an overview, we refer to [19]. However, in the spirit of explainability, and to reduce the risk of overfitting, we choose a simple

forecasting method which we describe next.

**Holt’s linear trend model.** We use Holt’s linear trend model to forecast the call volume of episode  $k$  using the realizations of previous episodes [19]. The forecast  $\hat{y}_i^{k+1}$  for the number of type- $i$  calls in episode  $k+1$  is the sum of the level estimate  $\ell_i^k$  and trend estimate  $b_i^k$ . The level estimate  $\ell_i^k$  is the weighted average of the actual number of calls during episode  $k$  and the forecast of the previous interval  $k-1$ , where the smoothing parameter  $\alpha \in [0, 1]$  controls the balance between reactivity to new data points and previous trends. Similarly, the trend estimate  $b_i^k$  is the exponentially smoothed moving average of the trend  $\ell_i^k - \ell_i^{k-1}$  with weight  $\beta \in [0, 1]$ . The update equations are given by:

$$\hat{y}_i^{k+1} = \ell_i^k + b_i^k, \quad (7)$$

$$\ell_i^k = \alpha y_i^k + (1 - \alpha) \hat{y}_i^{k-1}, \quad (8)$$

$$b_i^k = \beta (\ell_i^k - \ell_i^{k-1}) + (1 - \beta) b_i^{k-1}. \quad (9)$$

We initialize the forecast as  $\hat{y}_i^1 := 0$  for all  $i \in \mathcal{I}$ . The forecasted arrival rate  $\hat{\lambda}_i^{k+1}$  for type- $i$  customers for episode  $k+1$  is then the number of forecasted calls divided by the episode length  $h$ . Lastly, we take the maximum with zero since arrival rates cannot be negative:

$$\hat{\lambda}_i^{k+1} = \max\left(\frac{\hat{y}_i^{k+1}}{h}, 0\right). \quad (10)$$

It remains to choose suitable values for  $\alpha$  and  $\beta$ . To this end we analyzed the error between the forecast and the realizations of the training data for different values of  $\alpha$  and  $\beta$  and all customer types. Since the trend of the call volume differs per day and customer type, there is not one pair of values that outperforms all others. For  $\alpha$ , larger values lead to an overly reactive forecast that is sensitive to noise, while small values fail to pick up changes in the trend, which are especially present for type-1 customers. For balance, we therefore set  $\alpha = 0.5$  for the remainder of this paper. The larger  $\beta$ , the more sensitive the forecast is for rapid changes in the trend. However, most of the time, the trend changes only gradually. We therefore set  $\beta = 0.2$ .

Figure 3 shows the true call volumes against the estimates given by (7). Since the trend estimate (9) is based on exponentially smoothed historical data, we observe a lag in the forecast when the trend in the data suddenly changes: for example, the call volume of type-1 customers is underestimated during the sudden increase between 6am and 9am, and overestimated when the volume drops between 9am and 11am. Figure 4 analyzes the goodness-of-fit of Holt’s linear trend model using the Mean Absolute Scaled Error (MASE) measure, which is defined as  $1/n \sum_{k=1}^n |\hat{y}_i^k - y_i^k| / (1/(n-1) \sum_{\ell=2}^n |y_i^\ell - y_{i-1}^\ell|)$ , where  $n$  is the total number of intervals in a day. A MASE value less than 1 indicates that the forecast outperforms the 1-point rolling average ( $\hat{y}_i^k = y_i^{k-1}$ ). In Figure 4, we observe that Holt’s model outperforms the 1-point rolling average on most days, and the 3-point rolling average ( $\hat{y}_i^k = 1/3 \sum_{n=1}^3 y_i^{k-n}$ ) on all days. We conclude that Holt’s linear trend model does a reasonable job forecasting the customer arrival rate, and that it outperforms naive methods on most days.

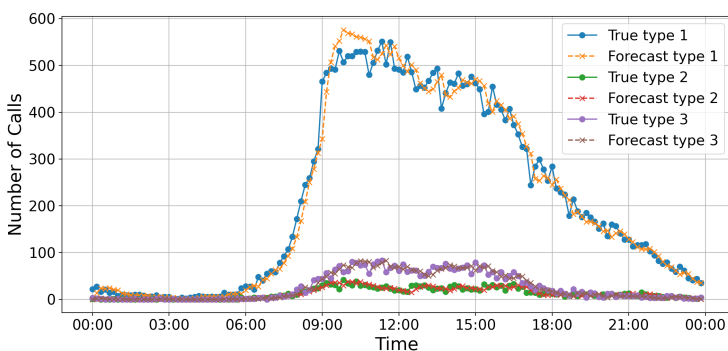


Figure 3: Forecast of the number of calls in 10-minute intervals for three different customer types on May 7, 2001 given by Holt’s linear trend model (7) with parameters  $\alpha = 0.5$  and  $\beta = 0.2$ .

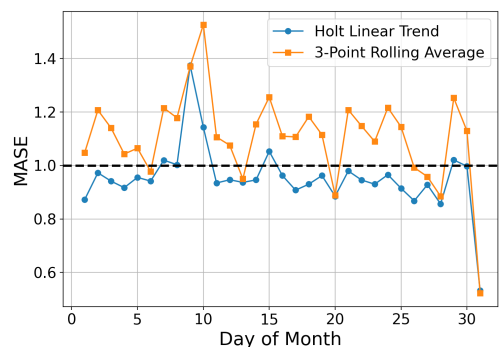


Figure 4: MASE of Holt’s linear trend model (7) and the 3-point rolling average for type-1 customers for May 2001. We note that May 9, 10, and 31 (Memorial Day) have an unusual arrival pattern.

## 4 Experiments

In this section we conduct experiments using our simulation framework to demonstrate the potential of Algorithm 1 (UCB-QR) in practical situations. In Section 4.1, we analyze the performance of UCB-QR against

commonly used benchmark routing policies. Since the results show significantly higher customer waiting times than the benchmarks, we introduce a new heuristic routing rule in Section 4.2 to replace Algorithm 2. With this, we show that the waiting times are successfully reduced and high payoffs are maintained. In Section 4.3, we discuss ways to adapt the UCB–QR algorithm to account for multiple objective functions and show an example where payoff maximization and server fairness are jointly optimized. Section 4.5 analyzes the sensitivity against estimation errors in the arrival and service rates and Section 4.6 tests the sensitivity of the algorithm’s performance to the episode length.

To analyze the performance of UCB–QR, we consider the following benchmark policies:

- **Oracle:** Similar to Algorithm 1, but with oracle knowledge of the payoff, arrival and service time parameters. In particular, this is Algorithm 1, but with replacing  $\hat{\theta}$ ,  $\hat{\lambda}$ , and  $\hat{\mu}$  in Line 5 and Line 7 by the actual  $\theta$ ,  $\lambda$ , and  $\mu$  as obtained from the data.
- **FCFS—ALIS:** If a server is idle and there are compatible customers waiting, assign the customer with the maximal waiting time. On the other hand, if there are idle compatible servers upon a customer arrival, assign it to the server with maximal idle time. This classical routing policy is widely used in practice since it is easy to implement and both customers and servers experience a sense of fairness [3].
- **Greedy:** If server  $j$  is idle and there are compatible customers waiting, assign the first-in-line customer with maximal expected payoff, i.e., a customer of type  $\operatorname{argmax}_{i \in \mathcal{I}} \theta_{ij}$ . If there are idle compatible servers upon a customer arrival, assign it to the server with maximal expected payoff  $\theta_{ij}$ . This policy maximizes the instantaneous payoff without considering long-term effects or stability constraints. Note that it depends on the true payoff parameter  $\theta$  and does not rely on  $\lambda$  and  $\mu$ .
- **Random:** If a server is idle and there are compatible customers waiting, choose a compatible queue uniformly at random and the first-in-line customer. If there are idle compatible servers upon a customer arrival, assign the customer to a compatible idle server uniformly at random. This policy serves as a most naive benchmark since it makes uninformed decisions.
- **$\theta\mu$  rule:** If server  $j$  is idle and there are compatible customers waiting, assign the first-in-line customer with maximal  $\theta_{ij}\mu_{ij}$ . If there are idle compatible servers upon a customer arrival, assign the customer to the server with maximal  $\theta_{ij}\mu_{ij}$ . This policy is a variation of the classical  $c\mu$  rule [5], which is known to be optimal for holding cost minimization in a multi-customer single-server setting, and has been well-studied in multi-customer multi-server settings [23, 24] and even in adaptive learning settings [7]. Instead of holding costs, we balance the average payoff  $\theta_{ij}$  with service speed  $\mu_{ij}$ .
- **Data:** We include the results from the data set which follow from the routing policy used by the call center. It is unknown to us which policy was applied.

## 4.1 Proof of concept

We apply UCB–QR on the data of June 2001. The pattern of arrivals, agent schedules, and the true value of  $\theta$  are given in B. We set the episode length to  $h = 2$  minutes and we take  $\varepsilon = 10^{-6}$  and  $p = 10^3$  in (1) and (2). Because the payoff parameters  $\theta_{ij}$  lie in  $[0, 1]$  and the penalty  $p$  is several orders of magnitude larger, giving weight to the variables  $x_{iz}$ ,  $i \in \mathcal{I}$  is discouraged and only happens when there is no other feasible solution. For each day and policy, we run 50 independent simulations with the same arrivals from the data.

**UCB–QR exhibits little day-by-day fluctuations** Figure 5 shows the average total payoff per day obtained by the different policies. The values are scaled by the value of the Oracle policy, i.e., the plot shows  $r_{\pi,i}/r_{O,i}$  where  $r_{\pi,i}$  is the average payoff for policy  $\pi$  on day  $i$ , and  $O$  indicates the Oracle policy. The call volume is different for each day, as shown in B, with fewer calls on weekends. The payoffs reflect the quality of the customer–server matches; higher values indicate better performance. Observe that the UCB–QR algorithm performs closely to the Oracle across all days. The loss in payoff due to learning  $\theta$  and estimating  $\lambda$  and  $\mu$  is 0.7 – 1% on week days and 1 – 2% during the weekend. The FCFS—ALIS, Random,  $\theta\mu$  policies and the policy from the data set obtain lower payoffs and show strong fluctuations over the month in contrast to the more stable performance of UCB–QR. Especially on June 25, most policies show a decrease in payoff except for UCB–QR. This showcases the potential of the algorithm to learn and adapt under different load patterns.

**Greedy sometimes performs best on weekends, but UCB–QR consistently reduces the optimality gap** Note that the differences in payoff accumulation in Figure 5 between the different policies are relatively small. For weekend days 3, 9, and 24 June, the Greedy policy, which is designed for myopic payoff maximization, achieves a higher payoff than UCB–QR. This can be explained by the value of the payoff parameter  $\theta$  (see e.g. Table 5 in B): the vector shows little variation over the different customer types and agent groups, especially for type-1 customers, while these customers dominate the call volume. We observe that in this case the Random policy performs quite well in terms of payoff and accumulates on average 96.5% of the Oracle payoff. The room for improvement is therefore small in this example: the optimality gap that measures the loss in payoff with respect to the Oracle payoff is just 3.5%. However, observe that the UCB–QR policy obtains on average 99.0% of the Oracle payoff, closing the optimality gap of the Random policy by approximately 71.4%.

**UCB–QR outperforms benchmarks under high variance payoffs** To gain a better insight in the payoff accumulation of UCB–QR, we conduct the same experiment using a transformed version of  $\theta$  that shows more variance over the different customer–agent combinations in C. The payoff accumulation in this case shows a clear benefit of UCB–QR over the benchmark policies and the policy of the data set: for all days, the UCB–QR policy achieves at least 98% of the Oracle payoff while other policies obtain as little as 60% on some days. Overall, the ordering of the policies is the same as in Figure 5, i.e., the Greedy and  $\theta\mu$  policies perform similarly and better than the FCFS–ALIS, Random, and Data policies. To conclude, UCB–QR achieves overall the best payoff accumulation, and the relative difference in payoff gain depends on  $\theta$ .

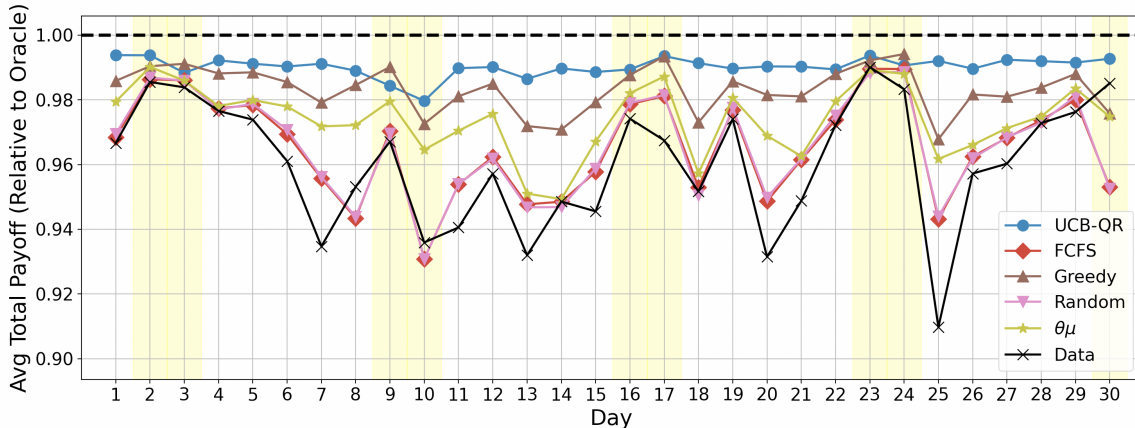


Figure 5: Average total payoff per day in June 2001 expressed relative to the Oracle policy, for Algorithm 1 (UCB–QR), the benchmark policies, as well as the (unknown) routing policy used in the data set. The variance from the average is negligible relative to the scale (10 compared to 50,000) and therefore omitted in the plot. The days highlighted in yellow are weekends.

**UCB–QR does not minimize waiting times** Figure 6 shows the waiting times of customers on June 4, and Figure 7 shows the average waiting times between 6am and 9pm (office hours). In the data set, there is a sharp peak in waiting time around midnight, while all other policies maintain more evenly distributed waiting times during the night. Around 6am, the offered load increases and many agents start their work. Between 6pm and 9pm the policy from the data set shows another peak, which is handled more smoothly by the Oracle policy and UCB–QR, indicating a better way of adapting to a change in load. The benchmark policies FCFS–ALIS, Greedy, Random, and  $\theta\mu$  consistently give low waiting times, which is why the plots are at some places indistinguishable. Overall, the waiting times for the UCB–QR and the Oracle policy are significantly higher than those of the benchmark policies and the policy used in the data set.

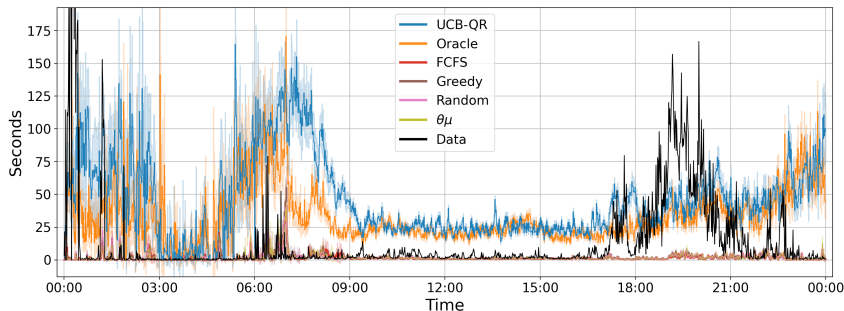


Figure 6: Average waiting times of customers over all classes with 95% confidence intervals, binned in 60 second intervals when applied to the data of June 4, 2001.

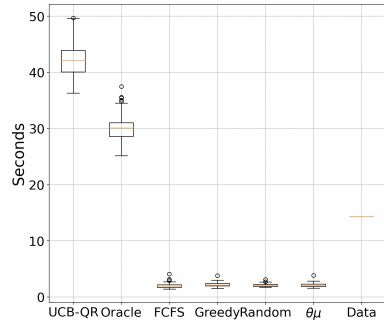


Figure 7: Boxplot of waiting time during office hours (6am-9pm) when applied to the data of June 4, 2001.

**Routing behavior of UCB-QR is affected by exploration** Figure 8 illustrates the total routing volume of customers to the different servers for UCB-QR and the Oracle policy, as well as the policy from the data set. UCB-QR routes customers similar to the Oracle policy, but deviations are due to learning the payoff parameter and estimating the arrival and service rates. The Oracle policy does not utilize server 26 at all, since the average payoffs for this server are lower than those at other servers (see B), and stability can be maintained without the capacity of this server. The UCB-QR policy does use server 26 since it needs to explore the different compatible lines. The Oracle policy routes type-1 customers mainly to server 1, while UCB-QR and the policy from the data set balances the load between servers 1 and 2. Server loads are further discussed in Section 4.3. Overall, we observe that exploration of the UCB-QR policy leads to different routing decisions when compared to the Oracle policy, although the overall payoff accumulation is competitive.

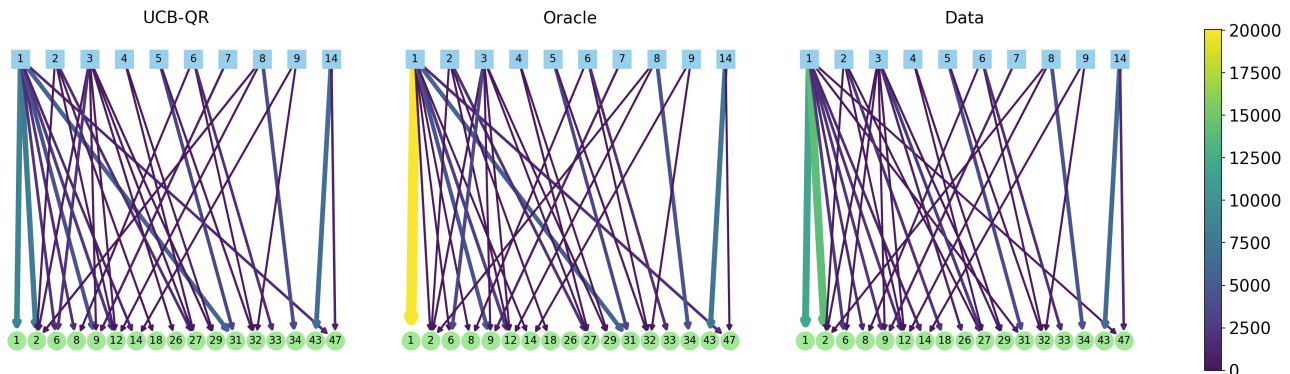


Figure 8: Routing volume for various routing policies when applied to the data of June 4, 2001.

**Computational complexity of UCB-QR matches benchmarks** All simulations were performed on separate threads using an Apple M1 Pro-chip with 8-core CPU. Running a full-day simulation of the UCB-QR algorithm takes about 20 seconds. Although this is twice as long as a typical runtime of roughly 10 seconds for the benchmark policies, it is still insignificant given that the simulation covers a 24-hour period.

## 4.2 Alternative routing rule to decrease waiting times

We now take a critical look at the routing rule Algorithm 2 used by UCB-QR and the Oracle policy. We note that Algorithm 2 is not very adaptive, since customers are assigned to a server (via the server’s virtual queue) upon arrival and are not allowed to be routed to another idling server even when the assigned server has a long virtual queue. Algorithm 2 also requires virtual queues which increases the complexity of the simulation, and the reshuffling of the virtual queues between episodes (Line 4) can be experienced as unfair from a viewpoint of both customers and servers in practice, since service is not FCFS (not even for customers of the same type) nor ALIS. We may therefore try to construct an improved routing rule with less delays, while still routing according to the desired rates described by the LP. Concretely, the empirical routing rates  $\mathbb{E}[D_{ij}(t)]/t$ , where  $D_{ij}(t)$  is the number of type- $(ij)$  departures up to time  $t$ , should converge to the desired rate  $x_{ij}$ . To the best of our knowledge, not many such rules exist in literature, since routing rates and even stability conditions are generally

difficult to determine for arbitrary routing rules for skill-based queues [2, 4].

Yet, it is more feasible to heuristically justify a routing policy that allocates customers in a matter that approximates the desired routing rates. To this end, we propose and test Algorithm 3, which takes inspiration from the heuristic JSQ- $K$  policy used in [16] (not to be confused with the JSQ- $K$  algorithm of [25]). Algorithm 3 takes as input routing rates  $x \in \mathbb{R}^{|\mathcal{L}|}$ , the maximizer of the LP (1) or (2) in case the former is infeasible, a payoff vector  $\theta \in \mathbb{R}^{|\mathcal{L}|}$ , and the episode length  $h$ . We stress that  $\hat{\theta}$  is used instead of the true value  $\theta$  in Algorithm 1. Each customer remains in the queue of its own type until it is assigned to an idle server, making virtual queues obsolete. Since the routing rate vector  $x$  is a BFS of an LP, it induces a spanning forest on the bipartite graph of customer types, servers, and compatibility lines  $(\mathcal{I} \cup \mathcal{J}, \mathcal{L})$  [16, Proposition 2], [17]. That is, the queues (consisting of customers of its own type) and servers are the nodes of the spanning forest and the edges are the queue-server connections with non-zero weight in the solution  $x$ . In such a forest, the parent and child nodes of servers are queues and *vice versa*. The root of the tree is a slack server, which has only child queues and no parent queue. This is possible since every tree in the spanning forest contains at least one slack server satisfying  $\sum_{(ij) \in \mathcal{L}} x_{ij} / \mu_{ij} < 1 - \varepsilon$ , and exactly one slack server if  $x$  is non-degenerate [16, Proposition 2]. Upon service completion, the server prioritizes customers of their child queue(s), and only if all child queues are empty, the server serves customers from its parent queue (if any). This way, non-slack servers are highly utilized, and the priority rule encourages routing decisions according to the target routing rates  $x$  corresponding to the spanning forest.

---

**Algorithm 3** Tree-based routing( $x, \theta, h$ ).

---

```

1: Consider the spanning forest of the bipartite graph  $(\mathcal{I} \cup \mathcal{J}, \mathcal{L})$  induced by  $x$ .
2: for time  $t = 0, \dots, h$  do ▷ Route customers.
3:   for each arrival of a type- $i$  customer at time  $t$  do
4:     if queue  $i$  has idling children servers in the spanning forest then
5:       Start service at the idle child server  $j$  that maximizes  $\theta_{ij}$ .
6:     else if the parent server of queue  $i$  is idle then
7:       Start service at the parent server.
8:     else
9:       Customer joins queue  $i$ .
10:    end if
11:  end for
12:  for each service completion at server  $j$  at time  $t$  do
13:    if server  $j$  has non-empty children queues then
14:      Start service of the first-in-line customer of the non-empty child queue  $i$  that maximizes  $\theta_{ij}$ .
15:    else if server  $j$  has a non-empty parent queue  $i$  then
16:      Start service of the first-in-line customer of the parent queue.
17:    else
18:      Server  $j$  remains idle.
19:    end if
20:  end for
21: end for

```

---

**Minimal payoff loss from heuristic routing rule** We compare the performance Algorithm 1 with an adapted version, called UCB-QR-Tree, which uses Algorithm 3 as routing rule instead of Algorithm 2. We found that the empirical routing volumes of customers to servers for UCB-QR-Tree were similar to those of UCB-QR, implying that the accumulated payoff is minimally effected as shown in Figure 9. By construction, we can intuitively argue that within each episode the empirical routing rates of Algorithm 3 should closely approximate their target  $x$ . Yet, from a small example in D it can be seen that the empirical routing rates  $\mathbb{E}[D_{ij}(t)]/t$  of Algorithm 3 do not converge to the target  $x_{ij}$  exactly, but only to values close to it. A theoretical analysis of the empirical routing rates remains a direction for future work. For a practical implementation, however, such minor deviations have little impact on performance measures including total payoff and waiting time, especially since there is inherent noise in the arrival and service rate estimators.

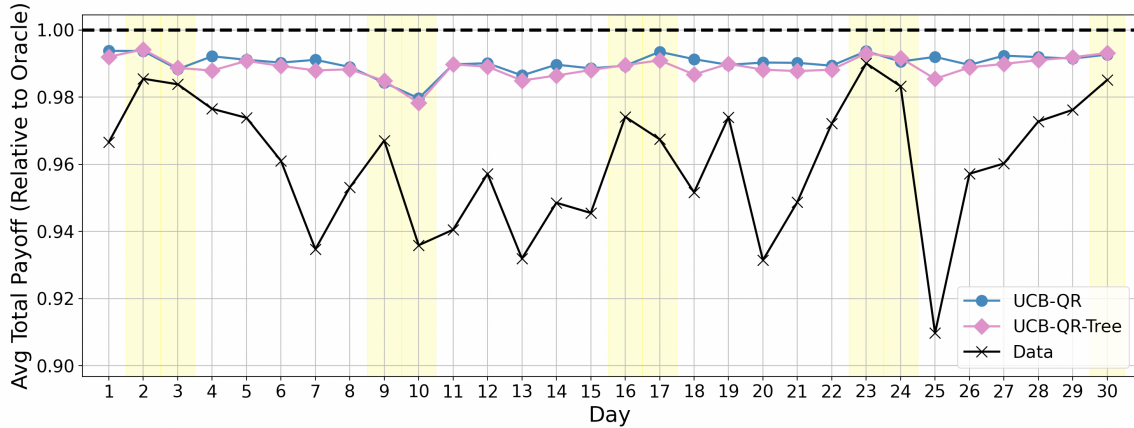


Figure 9: Average total payoff per day in June 2001 for the UCB-QR and UCB-QR-Tree policies.

**UCB-QR-Tree significantly reduces waiting times** The waiting times for UCB-QR-Tree are lower than those of UCB-QR, as shown in Figure 10. In Figure 10a, UCB-QR-Tree achieves waiting times almost as low as those of FCFS-ALIS. On the depicted day, the load is relatively low since there are many agents at work while the total call volume is moderate for a Monday (see Figure 19 and Figure 20 in B). However, on days with higher load the average delay of UCB-QR-Tree is slightly worse than FCFS-ALIS, although it still outperforms UCB-QR as shown in Figure 10b.

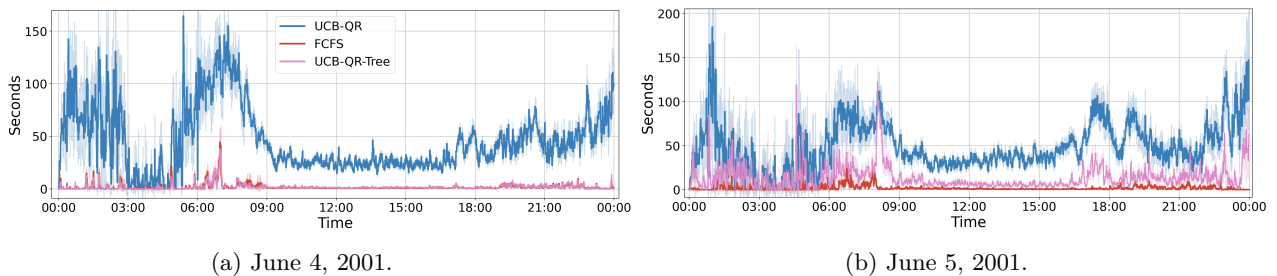


Figure 10: Average customer waiting time for the UCB-QR and UCB-QR-Tree policies.

**UCB-QR and UCB-QR-Tree have comparable runtimes** The computational complexity of UCB-QR-Tree is lower than UCB-QR, since virtual queues and reshuffling are omitted. However, at the start of each episode, the spanning forest must be determined based on the LP maximizer. The runtimes were not substantially affected in our specific experiments.

In conclusion, Algorithm 3 is an attractive alternative to Algorithm 2 for practical applications, where exact convergence to target routing rates is not crucial while low waiting times are. The UCB-QR-Tree policy still accumulates a similar high payoff as UCB-QR while waiting times are reduced significantly. It additionally promotes customer fairness in the sense of FCFS service for customers of the same type.

### 4.3 Combining different performance objectives

The UCB-QR algorithm is designed to maximize the total payoff, which is reflected in the objective function of (1). In practice, however, service system management typically accounts for multiple performance criteria simultaneously. Next, we demonstrate how the UCB-QR algorithm can be extended to cover other criteria as well, as long as they can be expressed in terms of routing rates  $x_{ij}$ ,  $(ij) \in \mathcal{L}$ . We first present an illustrative example that balances payoff maximization and server fairness, followed up by a discussion on how to achieve such integration for other objectives as well.

To balance payoff maximization and server fairness, we adapt the objective function of the LP (1) to account for fairness, see optimization problem (11). Here,  $\rho_j := \sum_{i \in \mathcal{I}} x_{ij} / \mu_{ij}$  represents the load of server  $j$ , and the penalty terms  $\rho_j - \bar{\rho}$  penalize deviation from the mean  $\bar{\rho} := 1/|\mathcal{J}| \sum_{j \in \mathcal{J}} \rho_j$ . The parameter  $\gamma \in \mathbb{R}$  controls the balance between server fairness and payoff maximization: the larger  $\gamma$ , the more weight is given to server fairness, at a cost of loss in payoff. Note that Algorithm 1 can simply be applied with this alternative optimization problem (11) replacing LP (1). For our simulation results next, we used the convex solver MOSEK [26].

$$\text{OPT}(\lambda, \mu, \theta, \varepsilon, \gamma) : \max_x \sum_{(ij) \in \mathcal{L}} \theta_{ij} x_{ij} - \gamma \sum_{j \in \mathcal{J}} (\rho_j - \bar{\rho})^2, \quad (11a)$$

$$\text{s.t.} \sum_{j \in \mathcal{S}_i} x_{ij} = \lambda_i, \quad \forall i \in \mathcal{I}, \quad (11b)$$

$$\sum_{i \in \mathcal{C}_j} \frac{x_{ij}}{\mu_{ij}} \leq 1 - \varepsilon, \quad \forall j \in \mathcal{J}, \quad (11c)$$

$$x_{ij} \geq 0, \quad \forall (ij) \in \mathcal{L}. \quad (11d)$$

**Load balancing decreases waiting times with minimal payoff loss** We observe in Figure 11 that the server loads indeed become more concentrated as the value of  $\gamma$  increases. As a result, the variance in the load per server also decreases. Here,  $\gamma = 0$  represents the original LP (1). This redistribution of work also affects customer waiting times: when more servers are actively involved in processing customers the system is less likely to develop long queues at critically loaded servers, which in turn reduces the overall waiting time as  $\gamma$  increases. However, because customers are not always matched to their highest payoff server, the total accumulated payoff becomes slightly lower. This trade-off is illustrated in Figure 12, which shows how increasing  $\gamma$  leads to shorter waiting times with only a modest decline in total payoff.

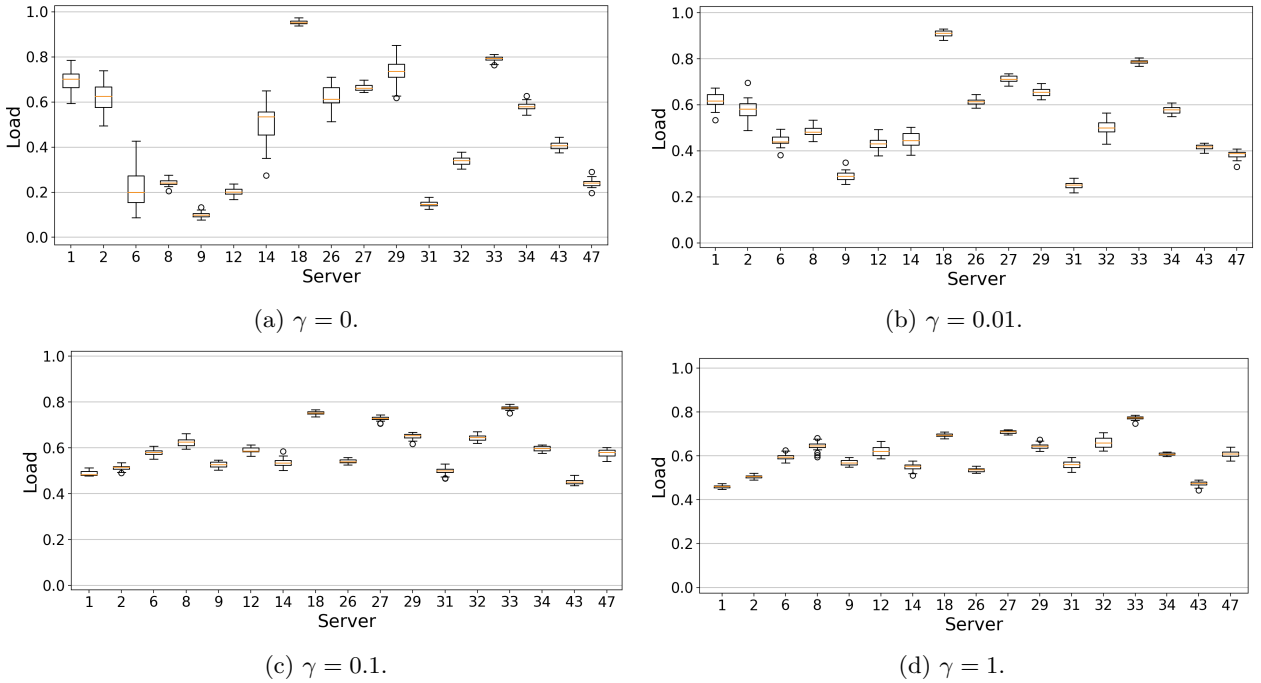


Figure 11: Empirical server load during office hours for UCB-QR with objective function (11) for different values of  $\gamma$  when applied to the data of June 4, 2001.

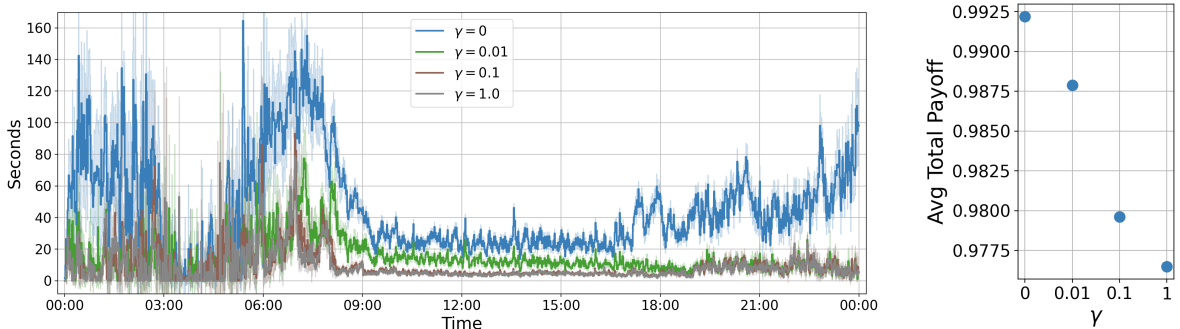


Figure 12: Average customer waiting time and average payoff (relative to the Oracle policy) of UCB-QR with objective function (11) for different values of  $\gamma$  when applied to the data of June 4, 2001.

**Incorporating other objectives** A similar approach can be used to integrate other objectives: we formulate a convex objective for the performance measure in terms of routing rates and add it with a trade-off parameter to the objective function in (2). Some examples are given in Table 2. Alternatively, bounds on the performance measures can be imposed by formulating new constraints for (2). For instance, server loads can be bounded using  $\delta_j \leq \rho_j \leq \bar{\delta}_j$  for  $\delta_j, \bar{\delta}_j \in [0, 1]$ .

Penalize critical server load	Penalize high waiting time	Penalize deviation from $x^0$	Encourage spare routing
$\sum_{j \in \mathcal{J}} \frac{1}{1-\rho_j}$	$\sum_{j \in \mathcal{J}} \frac{\rho_j}{1-\rho_j}$	$\sum_{(ij) \in \mathcal{L}} (x_{ij} - x_{ij}^0)^2$	$\sum_{(ij) \in \mathcal{L}} \log(1 + x_{ij})$

Table 2: Some examples of performance objectives expressed in terms of routing rates  $x_{ij}$ ,  $(ij) \in \mathcal{L}$ .

**Heuristic routing rule is incompatible with non-linear objectives** We note that routing rule Algorithm 3 is not implementable in its current form with a general optimization problem, since it relies on the properties of LPs. Specifically, it uses the spanning forest on the bipartite graph of customer types and servers induced by the optimal solution of the LP (1). This property, however, does not hold in general for convex optimization problems [17], hence we use Algorithm 2 in Algorithm 1.

#### 4.4 Resilience in bursty scenarios

We consider a day in the data set with relatively many customer arrivals and little available agents, namely December 31, 2001. We manually mimic three customer surges during office hours by adding artificial customer arrivals: we add 2,000 additional type-2 customer arrivals uniformly distributed between 10:00am and 10:10am, 2,000 type-3 arrivals between 11:00am and 11:10am, and 2,000 type-5 arrivals between 12:00pm and 12:10pm. The resulting bursty arrival process is shown in Figure 13. Since we found that UCB-QR can lead to high waiting times, we only consider UCB-QR-Tree in this experiment.

**Delayed recovery of UCB-QR-Tree after customer surges** We observe in Figure 14 that all policies show peaks in customer waiting times after the artificial incidents. The benchmark policies FCFS—ALIS, Greedy, Random, and  $\theta\mu$  recover quickly from the customer surges and return to the pre-surge level waiting times at approximately 12:30pm. However, the benchmark policies obtain overall lower payoff than UCB-QR-Tree, as shown in Table 3. The UCB-QR-Tree policy shows the highest peak in customer waiting time and recovers to pre-surge waiting time levels only at approximately 3pm. This behavior arises because the algorithm makes decisions based only on the arrival and service rate estimators for the current episode, without considering customers who are already waiting in the system. Since the surges occur in a small time interval, the arrival rate estimators recover quickly, and the routing scheme is chosen that optimizes the assignment of future customer arrivals, without considering the optimal assignment for the many customers in the system. We conclude that UCB-QR-Tree (and similarly UCB-QR) are not yet well-suited to handle bursty customer arrival processes, and further research it required. To address this, the episode length can be shortened or the values of  $\alpha$  and  $\beta$  in the arrival rate estimators (10) can be adjusted to make the routing algorithm more responsive to such customer surges. Alternatively, the LP (1) can be adapted to account for the number of customers of each type currently in the system.

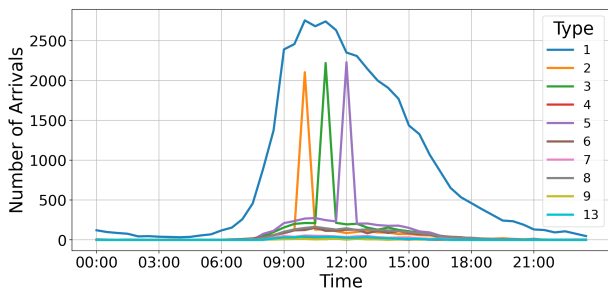


Figure 13: Customer arrivals with addition of the artificial bursty arrival process per 10-minute intervals for December 31, 2001.

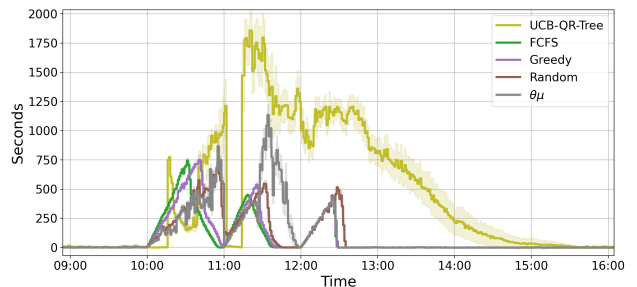


Figure 14: Average customer waiting time for different policies when applied to the modified arrival process on December 31, 2001.

UCB-QR-Tree	FCFS	Greedy	Random	$\theta\mu$
0.9910	0.9665	0.9883	0.9662	0.9811

Table 3: Average cumulative payoff relative to the Oracle policy.

## 4.5 Robustness against estimation errors

We analyze the sensitivity of UCB-QR to errors in arrival and service rate estimation. To this end, we compare four variations of Algorithm 1. The algorithms follow the same steps as described in Algorithm 1, but differ in the knowledge of system parameters.

- $(\hat{\theta}, \hat{\lambda}, \hat{\mu})$  UCB-QR, which uses UCB estimators  $\hat{\theta}$ , estimators  $\hat{\lambda}$  in (10) for the arrival rates, and empirical estimators  $\hat{\mu}$  in (6) for the service rates.
- $(\theta, \lambda, \mu)$  Oracle, which uses the true values  $\theta, \lambda, \mu$ .
- $(\hat{\theta}, \hat{\lambda}, \mu)$  UCB-QR- $\mu$ , which uses UCB estimators  $\hat{\theta}$  and estimators  $\hat{\lambda}$  in (10), but the true service rates  $\mu$ .
- $(\hat{\theta}, \lambda, \hat{\mu})$  UCB-QR- $\lambda$ , which uses UCB estimators  $\hat{\theta}$ , the true arrival rates  $\lambda$ , and empirical estimators  $\hat{\mu}$  in (6) for the service rates.

**Estimation error in arrival and service rates has little impact** We found that both variants UCB-QR- $\mu$  and UCB-QR- $\lambda$  perform close to UCB-QR in terms of payoff accumulation. By granting access to the true arrival rate or service rate, the cumulative payoff is only increased in the order of 0.1%. Next to that, the average waiting times are comparable, as shown in Figure 15. We conclude that the algorithm’s performance can only be slightly improved in practice by reducing the estimation errors in the arrival and service rates.

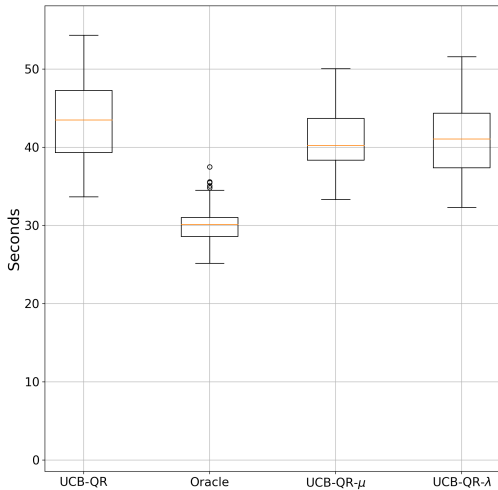


Figure 15: Boxplot of waiting time during office hours for different variants of UCB-QR relying on different system information when applied to the data of June 4, 2001.

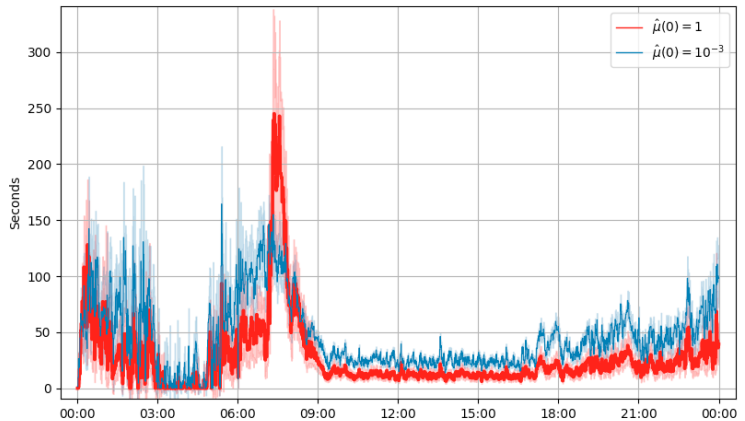


Figure 16: Average waiting time of UCB-QR for two different initial values of the empirical estimators  $\hat{\mu}$ . Overestimation of  $\hat{\mu}$  leads to a significant peak in waiting times around 7am.

**Additional exploration bonus can lead to system instability** We note that UCB-QR uses UCB estimators for the average payoff, but empirical estimators for the service rates. One might wonder whether adding further exploration bonus to the service rate estimators could improve the algorithm’s performance. In UCB-QR, the service rate estimators are initialized at a small value ( $10^{-3}$ ), deliberately underestimating their true mean. We find that when  $\hat{\mu}$  overestimates its true mean, the average customer waiting time experiences a significant peak during the start of office hours, as shown in Figure 16. This can be explained as follows. During the low traffic night hours, not all compatible connections have been explored yet, so most estimators  $\hat{\mu}_{ij}$  are still at the initial value at the start of office hours. The solution of the optimization problem (1) is then to route a large amount of customers to one server, much more than its true capacity. As a result, the size of one virtual queue is large, while other servers are idling. Of course, the empirical estimators are updated after each episode so the algorithm does recover after a few episodes. We observe in Figure 16 that the algorithm with high initial values even performs better in terms of waiting time after the morning peak, since more compatible lines are used that are not explored by the algorithm with small initial values. However, since the errors are made during the high traffic morning peak, the overall average waiting time suffers from overestimation of  $\hat{\mu}$ : we found that with small initial values, the average waiting time during office hours is approximately 44

seconds, and 58 seconds with large initial values. We found that the cumulative payoff is not noticeably affected.

To conclude, on this realistic data set, the performance of the UCB-QR algorithm is not greatly improved by increasing the accuracy of the  $\hat{\lambda}$  and  $\hat{\mu}$  estimators. Adding an exploration bonus to the service rate estimators can be beneficial for exploration, but it can lead to an increase in waiting times when the traffic becomes large while not yet all lines have been used.

## 4.6 Balancing reactivity and complexity

We analyze the sensitivity of our results with respect to the episode length  $h$  used by UCB-QR in Line 2. The shorter the episode, the faster the payoff parameters  $\theta$  are learned, and the faster the algorithm reacts to changes in arrival rates. At the same time, it also increases computational complexity since an optimization problem is solved and the virtual queues are reshuffled each episode (Line 5 in Algorithm 1 and Line 2-4 in Algorithm 2).

**Large  $h$  leads to significant delays** We observe in Table 4 that for an episode length exceeding 10 minutes, the episode updates are no longer the dominant factor in computation complexity, since runtime no longer decreases when increasing episode lengths. Moreover, the cumulative payoff is not very sensitive to the episode length, where larger episodes give slightly higher payoff since there is less noise in the estimators. Customer waiting times, however, are less robust: the average waiting time in Figure 17 increases with the value of  $h$ . Especially the morning and evening hours are chaotic with large peaks in waiting times, since the algorithm is not able to pick up changes in traffic volume adequately fast. Hence,  $h$  should be chosen small enough to capture changes in time-varying arrival rates.

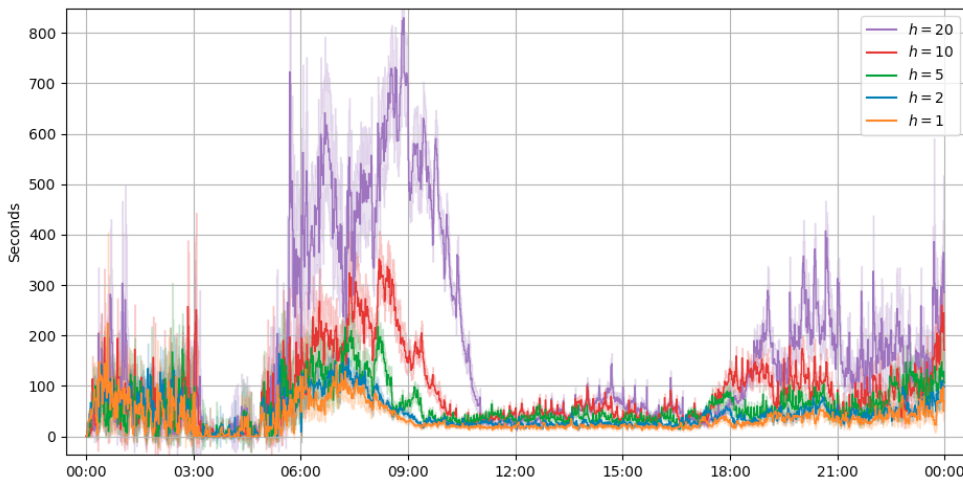


Figure 17: Average customer waiting time of the UCB-QR algorithm for different values of the episode length  $h$  (min) when applied to the data of June 4, 2001.

$h$	Runtime	Payoff
1	48	0.9914
2	30	0.9922
5	20	0.9931
10	17	0.9934
20	17	0.9922

Table 4: Average runtime in seconds and the average cumulative payoff relative to the Oracle policy of the UCB-QR algorithm for different values of the episode length  $h$  (min) when applied to the data of June 4, 2001.

## 5 Conclusion

We have demonstrated the effectiveness of the reinforcement learning algorithm UCB-QR in a practical setting using real-world data, serving as a concrete step towards live implementation of learning-based control policies in real-life skill-based queueing systems. We briefly summarize our findings. We have shown that UCB-QR effectively learns the payoff parameters in realistic time-varying environments while its practical computational complexity was comparable with those of benchmark static policies such as FCFS—ALIS and the  $c\mu$  rule. Moreover, we have shown that customer waiting times can be drastically reduced with only a minor loss in payoff by using a more efficient heuristic routing rule (Algorithm 3). The algorithm can be easily extended to allow for multiple objectives: we have illustrated by example the joint optimization of payoff accumulation and server fairness, where a tuning parameter is used to balance the trade-off. In case of sudden customer surges, we observed that UCB-QR does not recover to the pre-surge performance as quickly as benchmark policies. To improve robustness against such bursty arrival processes however, better finetuning of the algorithm parameters is required. We found that for this data set, not much can be gained in terms of payoff or customer delay by reducing the noise in arrival and service rate estimators. Lastly, we have shown that the episode length as parameter of the UCB-QR algorithm requires careful tuning depending on the application to maintain short customer delays.

For this study we used a public data set of call center logs from 2001 to 2003, although a case study for different applications, such as data centers or cloud computing networks, with more recent data would be useful follow-up research for practice. Other possible directions for future research include considering applications with customer abandonments, increasing adaptability of the algorithm by using event-based updates rather than episodes, and generalizing for multi-pool systems.

## **Acknowledgments**

This work is part of *Valuable AI*, a research collaboration between the Eindhoven University of Technology and the Koninklijke KPN N.V. Parts of this research have been funded by the EAISI's IMPULS program, and by Holland High Tech — TKI HSTM via the PPS allowance scheme for public-private partnerships.

## References

- [1] Jinsheng Chen, Jing Dong, and Pengyi Shi. A survey on skill-based routing with applications to service operations management. *Queueing Systems*, 96(1-2):53–82, 2020.
- [2] Ivo Adan and Gideon Weiss. Exact FCFS matching rates for two infinite multitype sequences. *Operations Research*, 60(2):475–489, 2012.
- [3] Ivo Adan and Gideon Weiss. A skill-based parallel service system under FCFS-ALIS — steady state, overloads, and abandonments. *Stochastic Systems*, 4(1):250–299, 2014.
- [4] Gideon Weiss. *Scheduling and Control of Queueing Networks*. Cambridge University Press, Cambridge, 2021.
- [5] Wayne E. Smith. Various optimizers for single-stage production. *Naval Research Logistics Quarterly*, 3:59–66, 1956.
- [6] Yueyang Zhong, John R. Birge, and Amy Ward. Learning the scheduling policy in time-varying multiclass many server queues with abandonment. *SSRN Electronic Journal*, (2012), 2022.
- [7] Subhashini Krishnasamy, Ari Arapostathis, Ramesh Johari, and Sanjay Shakkottai. On learning the  $c\mu$  rule in single and parallel server networks. *2018 56th Annual Allerton Conference on Communication, Control, and Computing, Allerton 2018*, pages 153–154, 2018.
- [8] Virag Shah, Lennart Gulikers, Laurent Massoulié, and Milan Vojnović. Adaptive matching for expert systems with uncertain task types. *Operations Research*, 68(5):1403–1424, 2020.
- [9] J. G. Dai and Mark Gluzman. Queueing Network Controls via Deep Reinforcement Learning. *Stochastic Systems*, 12(1):30–67, 2022.
- [10] Chen Tessler, Yuval Shpigelman, Gal Dalal, Amit Mandelbaum, Doron Haritan Kazakov, Benjamin Fuhrer, Gal Chechik, and Shie Mannor. Reinforcement Learning for Datacenter Congestion Control. *SIGMETRICS Performance Evaluation Review*, 49(2):43–46, 2022.
- [11] Sisheng Liang, Zhou Yang, Fang Jin, and Yong Chen. *Data Centers Job Scheduling with Deep Reinforcement Learning*, volume 12085 LNAI. Springer International Publishing, 2020.
- [12] Céline Comte, Matthieu Jonckheere, Jaron Sanders, and Albert Senen-Cerda. Score-Aware Policy-Gradient Methods and Performance Guarantees using Local Lyapunov Conditions: Applications to Product-Form Stochastic Networks and Queueing Systems. *ArXiv: 2312.02804*, 2023.
- [13] Sanne van Kempen, Jaron Sanders, Fiona Sloothaak, and Maarten G Wolf. Learning payoffs while routing in skill-based queues. *ArXiv: 2412.10168*, 2024.
- [14] Peter Auer, Nicolò Cesa-Bianchi, and Paul Fischer. Finite-time analysis of the multiarmed bandit problem. *Machine Learning*, 47(2-3):235–256, 2002.
- [15] Tor Lattimore and Csaba Szepesvári. *Bandit Algorithms*. Cambridge University Press, Cambridge, 2020.
- [16] Xinzhe Fu and Eytan Modiano. Joint learning and control in stochastic queueing networks with unknown utilities. *Proceedings of the ACM on Measurement and Analysis of Computing Systems*, 6(3), 2022.
- [17] Dimitris Bertsimas and John N. Tsitsiklis. *Introduction to Linear Optimization*. Athena scientific, Belmont, MA, 1997.
- [18] Joel E. Cohen and Frank P. Kelly. *Reversibility and Stochastic Networks*, 1981.
- [19] Robin John Hyndman and George Athanasopoulos. *Forecasting: Principles and Practice*. OTexts, Melbourne, 2021.
- [20] Andrea Bastianin, Marzio Galeotti, and Matteo Manera. Statistical and economic evaluation of time series models for forecasting arrivals at call centers. *Empirical Economics*, 57(3):923–955, 2019.
- [21] Y. Goldberg, Y. Ritov, and A. Mandelbaum. Predicting the continuation of a function with applications to call center data. *Journal of Statistical Planning and Inference*, 147:53–65, 2014.
- [22] Nadja Klein. Distributional Regression for Data Analysis. *Annual Review of Statistics and its Application*, 11(1):321–346, 2024.

- [23] Li Xia, Zhe George Zhang, and Quan Lin Li. A  $c/\mu$ -Rule for Job Assignment in Heterogeneous Group-Server Queues. *Production and Operations Management*, 31(3):1191–1215, 2022.
- [24] Zhenghua Long, Hailun Zhang, Jiheng Zhang, and Zhe George Zhang. The Generalized  $c/\mu$  Rule for Queues with Heterogeneous Server Pools. *Operations Research*, 72(6), 2023.
- [25] A. Ephremides, P. Varaiya, and J. Walrand. A Simple Dynamic Routing Problem. *IEEE Transactions on Automatic Control*, 25(4):690–693, 1980.
- [26] MOSEK ApS. MOSEK Optimizer API for Python. (January), 2023.
- [27] C. G. Cassandras and S. Lafortune. *Introduction to discrete event systems*. Springer, Boston, MA, 2008.

# A Data and simulation description

	call_id	cust_subcall	record_id	node	service	first_service	segment_start	segment_end	seg_type	outcome	seg_parties	wait_time	queue_time	service_time	party_answered	agent_group	main_service
0	486000002	1	4	2	1	1	2001-05-01 00:00:48	2001-05-01 00:03:35	3	1	20	0	0	167	26512	9	7
1	486000009	1	12	2	1	1	2001-05-01 00:00:14	2001-05-01 00:00:26	3	2	20	1	1	11	26969	2	1
2	486000010	1	15	2	1	1	2001-05-01 00:01:26	2001-05-01 00:03:17	3	1	20	2	2	108	26475	11	1
3	486000021	1	32	2	1	1	2001-05-01 00:00:52	2001-05-01 00:03:45	3	1	20	0	0	173	26488	2	1
4	486000025	1	37	3	1	1	2001-05-01 00:00:28	2001-05-01 00:04:38	3	1	20	1	1	249	38253	2	1

Figure 18: Excerpt of the call log table of the data set. Here, “outcome” encodes the reason why the call ended, such as abandonment or transfer, and “party\_answered” is the id of the agent that answered the call.

The data set contains 130 gigabytes of tables with detailed information about call logs and agent shifts from a U.S. bank call center over the period from April 2001 to October 2003. An example of such call logs is shown in Figure 18. The call center operates 24 hours a day, 7 days a week. On an average weekday, approximately 1.200 agents handle around 50.000 calls. Calling customers are processed by a Voice Response Unit (VRU) which determines the type of service requested by the customer. We label the different service requests as customer types. Not all customer types appear in each month of the data. In May, June, and November 2002, new services were introduced by the call center’s management, bringing the total to 17 different customer types.

Service in the call center of the data set is skill-based. The agents are partitioned into 47 different groups based on their service capabilities. The data set contains detailed information about the agents’ work hours, calling times, and idle times.

## A.1 Data preparation

Since the service categories and the agent populations change over time, we consider the compatibility between customer types and agent groups per month. For a given month, we define a customer type and agent group to be *compatible* if there are at least 100 calls of that combination within the month. An example of the customer types, agent groups and their compatibility is given in B. In the data set, at most 1% of the customers abandon the system before speaking to an agent. We neglect these relatively rare abandonments and only consider calls where the customer interacts with an agent. Within one month, about 3% of the customers interact with more than one agent, either due to call transfers or multiple calls initiated by the customer. For simplicity, we neglect this aspect and treat each call independently as a unique customer.

## A.2 Simulation description

For this study we created a discrete-event simulation to model a general multi-class, multi-server queueing system with customer–server compatibility constraints. In short, the simulation framework is described as follows.

**Input.** To run the simulation, one has to specify the queueing system’s configuration including the number of customer types, the number of servers, and the compatibility relations between customers and servers. For each customer type an efficient list structure (deque) is created. Next to that, we create a Server object for each server that stores its id number and status (idle, busy, or inactive). For each compatible customer–server pair, a payoff distribution has to be specified. For the arrival process, either a list of customer arrival times or an interarrival distribution is required. For the service distributions, the simulation supports both server dependent and customer–server dependent distributions. Optionally, an agent schedule can be provided that specifies the number of active agents at certain timestamps.

**Simulation dynamics.** The simulation follows a discrete-event approach [27]: future events are stored in an event queue and the simulation progresses by repeatedly processing the next scheduled event. Events can be of the type arrival, departure, agent schedule update, or episode end. Upon an arrival, the customer is allocated to either an idle server, or a (virtual) queue according to the routing policy. Upon a service completion, a payoff is sampled according to the payoff distribution of the customer–server pair, empirical estimators for the service duration and average payoff are updated, and the next service completion is scheduled if there are customers in the queues allocated to this server. Otherwise, the server status is set to idle.

**Simulation output.** The simulation output is an event log containing details (time stamp, customer type and id, server id) of all events including arrivals, the start of services, and service completions. From the event log, key performance indicators such as average payoff, customer waiting times, server utilization, and queue lengths are obtained. Each simulation is ran multiple times to reduce the fluctuations in the randomly sampled arrival times (unless the arrivals are specified according to a deterministic list), service times, and payoffs.

## B Input data of the first week of June 2001

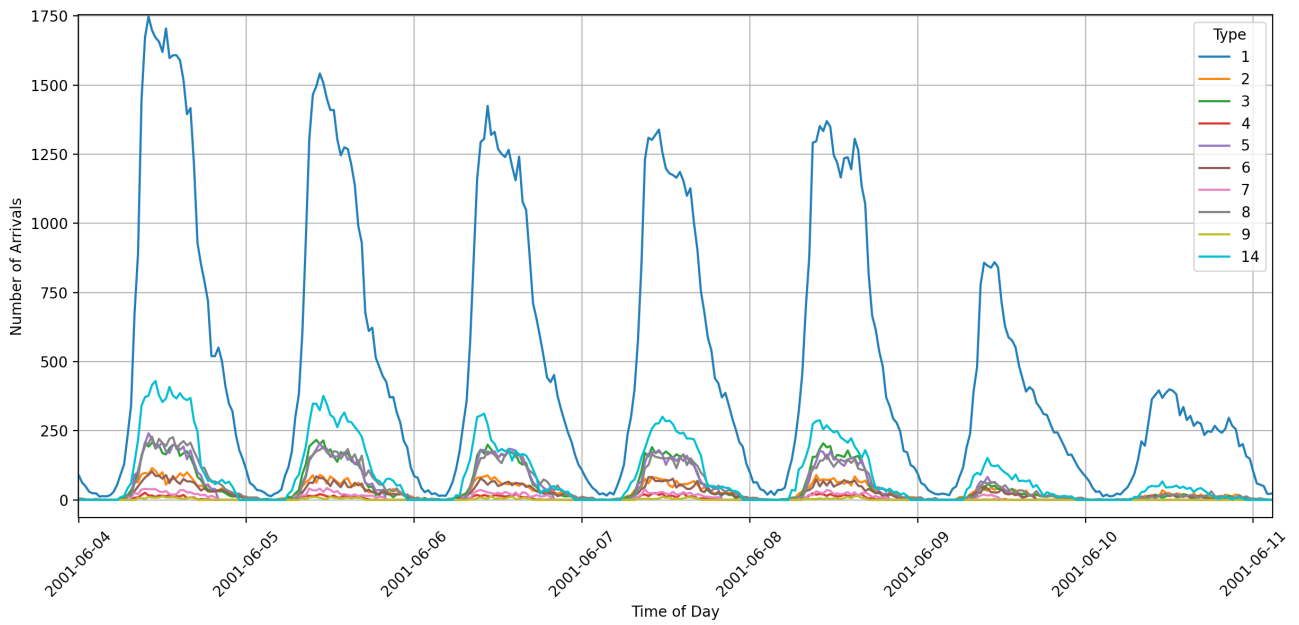


Figure 19: Number of customer arrivals per type accumulated per 30-minute intervals for the first week of June 2001.

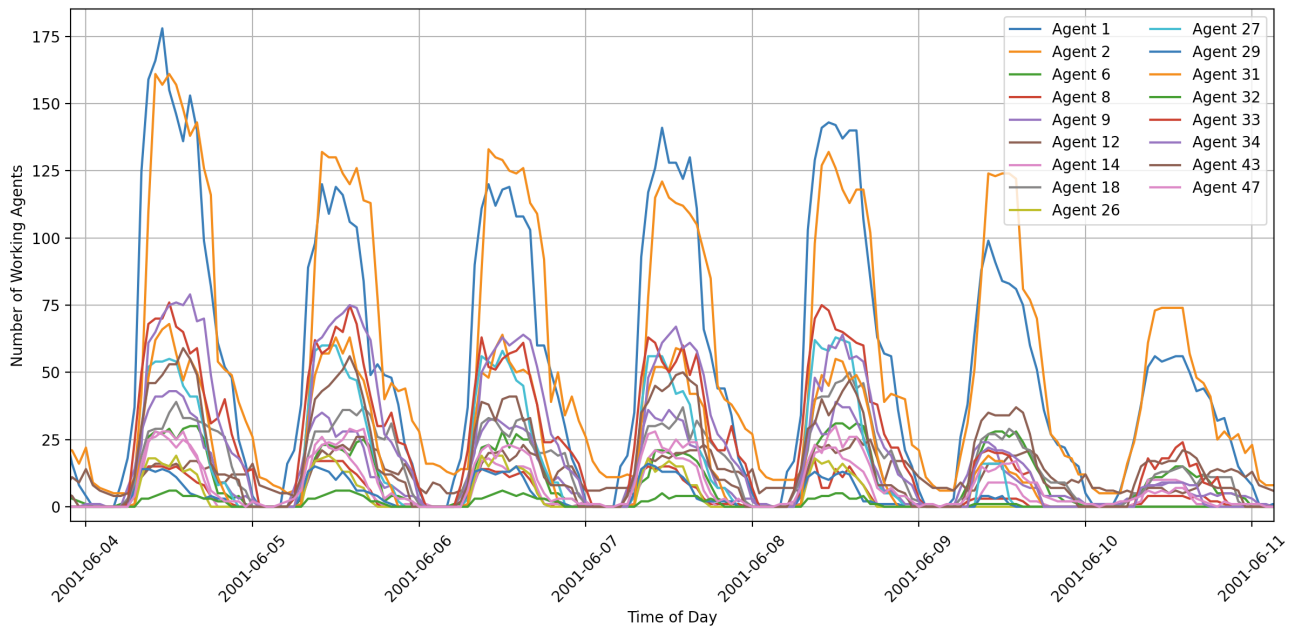


Figure 20: Number of working agents per group accumulated per hour for the first week of June 2001. Here, working means being available to answer calls. Most agents are active between 6am and 9pm.

Agent \ Customer	Customer										
	1	2	3	4	5	6	7	8	9	14	
1	0.84										
2	0.84	0.82	0.93					0.67			
6	0.81		1.00								
8	0.84					0.71					
9	0.87		0.89				0.97				
12	0.85	0.89	0.84					0.61			
14	0.80								0.69		
18		0.86									
26			0.90								
27		1.00	0.90	1.00							
29			0.91	0.91							
31	0.88				0.84						
32					0.84	0.69			0.90		
33						0.86					
34								0.78			
43											0.95
47	0.92										0.96

Table 5: True value of the payoff parameter  $\theta_{ij}$  for all lines  $(ij) \in \mathcal{L}$  for 4 June 2001.  $\theta_{ij}$  is the fraction of successful  $(ij)$  calls in the data set on this day, i.e., calls that are not transferred nor end in a conference. An empty cell means that the customer-agent pair is incompatible.

## C Adapted payoff value

We consider the same setting as Section 4.1, but use an adapted payoff parameter  $\theta'$ . We normalize the values  $\theta_{ij}$  to the range  $[0, 1]$  and apply a power transformation to increase the relative differences. Concretely, we define

$$\theta'_{ij} = \sqrt{\frac{\theta_{ij}}{\max_k \theta_{ik} - \min_\ell \theta_{i\ell}}}, \quad (12)$$

for customer types  $i \in \mathcal{I}$  with more than one compatible line, and  $\theta'_{ij} = \sqrt{\theta_{ij}}$  for customer types with only one connection. For example, the adapted value  $\theta'$  for June 4 2001 is shown in Appendix C, which shows much more variation than the original value of  $\theta$  (Table 5 in B).

Agent \ Customer	Customer										
	1	2	3	4	5	6	7	8	9	14	
1	0.60										
2	0.59	0.00	0.76					0.59			
6	0.37		1.00								
8	0.58					0.40					
9	0.76		0.54				0.98				
12	0.69	0.61	0.00					0.00			
14	0.00								0.00		
18		0.45									
26			0.61								
27		1.00	0.58	1.00							
29			0.65	0.00							
31	0.84				1.00						
32					0.00	0.00			1.00		
33						1.00					
34								1.00			
43											0.00
47	1.00										1.00

Table 6: Adapted value of  $\theta'$  according to (12) for 4 June 2001.

Consequently, we run the same simulation as described in Section 4.1, but now using  $\theta'$ . The average payoff is shown in Figure 21.

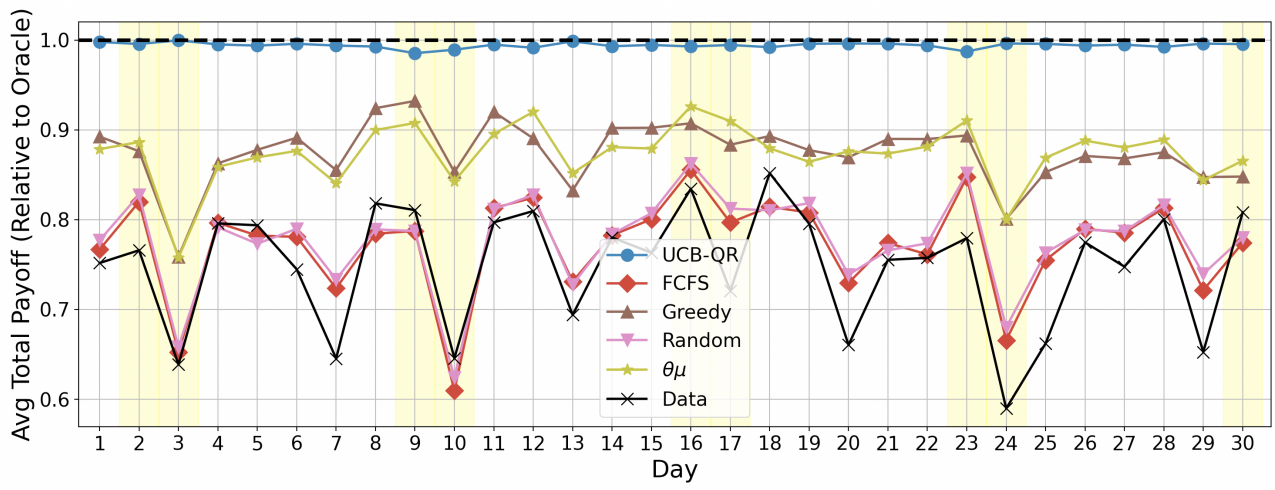


Figure 21: Average total payoff per day in June 2001, expressed relative to the Oracle policy, based on the adapted payoff parameter  $\theta'$  in (12).

## D Performance of Algorithm 3 on a small example

Consider a queueing system with  $I = 3$  customer types and  $J = 3$  servers, and full compatibility  $\mathcal{L} = \{(i, j) \mid \forall i \in \mathcal{I}, j \in \mathcal{J}\}$  as shown in Figure 22. Arrivals of type- $i$  occur according to independent Poisson processes with rate  $\lambda_i$  and type- $(ij)$  service times are independent and exponentially distributed with rate  $\mu_{ij} = \mu_j$  for all  $i \in \mathcal{I}$  and  $j \in \mathcal{J}$ .

We consider the following non-degenerate BFS of (1),

$$x_{11} = \mu_1 - \varepsilon = 1 - \varepsilon, \quad (13a)$$

$$x_{12} = \lambda_1 - x_{11} = 2 + \varepsilon, \quad (13b)$$

$$x_{22} = \mu_2(1 - \varepsilon) - x_{12} = 3 - 6\varepsilon, \quad (13c)$$

$$x_{23} = \lambda_2 - x_{22} = 4 + 6\varepsilon, \quad (13d)$$

$$x_{32} = \lambda_3 = 5. \quad (13e)$$

In this case, server 3 has slack, since (1c) is not binding. The spanning forest induced by  $x$  is shown in Figure 23.

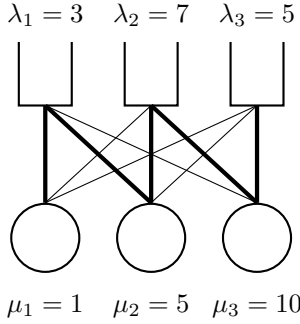


Figure 22: Queueing system with full compatibility. The lines with non-zero mass in  $x$  in (13) are shown in bold.

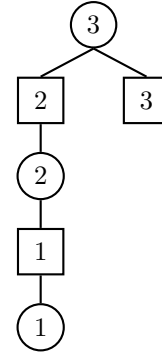


Figure 23: Spanning forest induced by  $x$  in (13). Here, customer types are represented by squares and servers by circles. Server 3 is the root since it has slack.

We apply the routing rule Algorithm 3 to route customers according to the rates (13). The results are based on 100 independent simulations with a runtime of 500 time units, and episode lengths  $h = 10$ . Figure 24 shows the running average empirical routing rates. After 500 time units, the routing rates have converged to approximately

$$\frac{D_{11}(t)}{t} \approx 0.863, \quad \frac{D_{12}(t)}{t} \approx 2.153, \quad \frac{D_{22}(t)}{t} \approx 2.649, \quad \frac{D_{23}(t)}{t} \approx 4.338, \quad \frac{D_{33}(t)}{t} \approx 5. \quad (14)$$

There does not exist a value of  $\varepsilon > 0$  such that the empirical routing rates agree with the analytical solution (13). Hence, the routing rates converge approximately, but not exactly to the target  $x$ .

Next to that, the server loads according to the analytical solution (13) are given by  $\rho_1 = x_{11}/\mu_1 = 1 - \varepsilon$ ,  $\rho_2 = (x_{12} + x_{22})/\mu_2 = 1 - \varepsilon$ , and  $\rho_3 = (x_{23} + x_{33})/\mu_3 = (9 + 6\varepsilon)/10$ . However, we find that the empirical server loads converge to approximately (see Figure 25)

$$\frac{W_1(t)}{t} \approx 0.852, \quad \frac{W_2(t)}{t} \approx 0.955, \quad \frac{W_3(t)}{t} \approx 0.936, \quad (15)$$

where  $W_j(t)$  is the total amount of time server  $j$  has been working (not idling) up to time  $t$ . This does not match the analytical solution  $\rho$ , since e.g.  $\rho_1 = \rho_2$  but  $W_1(t)/t \neq W_2(t)/t$ .

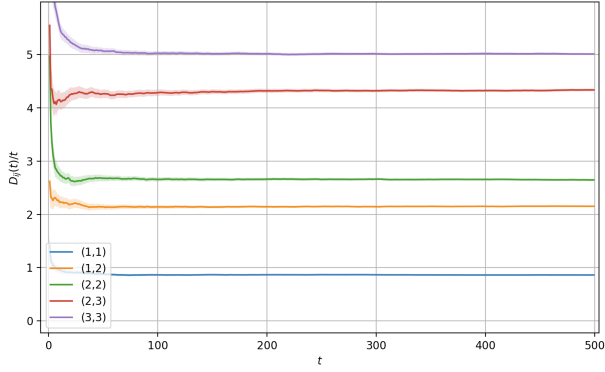


Figure 24: Empirical routing rates  $D_{ij}(t)/t$  over time  $t$  for the different lines  $(ij)$ .

To analyze the difference in performance between the routing rules Algorithm 2 and Algorithm 3, we run the UCB-QR, UCB-QR-Tree, and the Oracle policy for the queuing system as shown in Figure 22. The cumulative payoff is shown in Figure 26 and the average customer waiting time in Figure 27. The UCB-QR and UCB-QR-Tree algorithms obtain a very similar payoff rate. For both UCB-QR and the Oracle policy, customers waiting times exhibit sharp peaks at new episodes, i.e., every  $h = 10$  time units. This is an effect of Algorithm 2: customers are redistributed amongst the virtual queues at the start of each new episode, and therefore customers that have been waiting for some time are suddenly at the head of the virtual queue and start service. The waiting times under UCB-QR-Tree are significantly lower than those of UCB-QR and the Oracle policy, showing that Algorithm 3 is more efficient in customer routing than Algorithm 2, with only a slight loss in payoff.

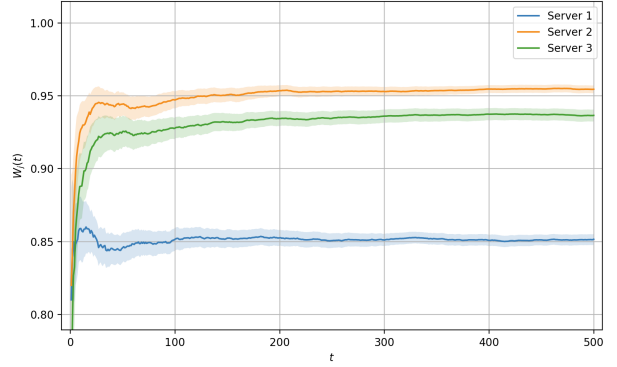


Figure 25: Empirical server load  $W_j(t)/t$ .

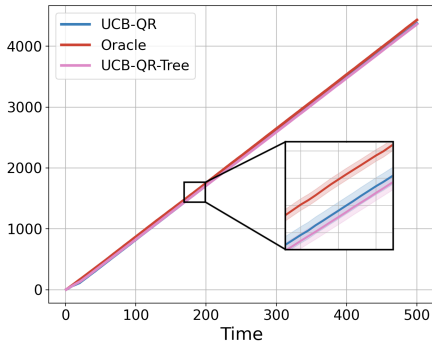


Figure 26: Cumulative payoff.

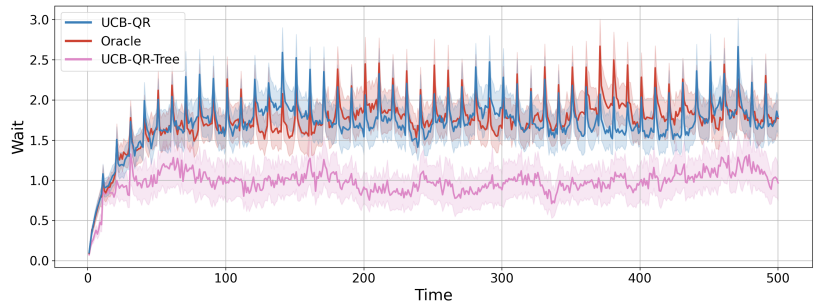


Figure 27: Average customer waiting time.